Antenna and Radar Front-End Design for Heartbeat Detection for Triggering Purposes of Medical Devices

Ronny Hahnel
Chair for RF Engineering
Dresden University of Technology
01062 Dresden, Germany
ronny.hahnel@tu-dresden.de

Mario Schiselski
Chair for RF Engineering
Dresden University of Technology
01062 Dresden, Germany
mario.schiselski@tu-dresden.de

Martin Laabs
Chair for RF Engineering
Dresden University of Technology
01062 Dresden, Germany
martin.laabs@tu-dresden.de

Qiong Wang
Chair for RF Engineering
Dresden University of Technology
01062 Dresden, Germany
qiong.wang@tu-dresden.de

André Henning
Institute for Biomedical Engineering
Dresden University of Technology
01062 Dresden, Germany
andre.henning@mailbox.tu-dresden.de

Dirk Plettemeier
Chair for RF Engineering
Dresden University of Technology
01062 Dresden, Germany
dirk.plettemeier@tu-dresden.de

ABSTRACT

This paper presents a single patch antenna design operating in 868 MHz band. The antenna is integrated in a mat for the human heartbeat detection, which in turn is used for triggering purposes of medical devices. To broaden the operating bandwidth so that the variation of the electrical properties from different patients can be neglected, a U-shape is slotted on the radiation patch and moreover a thick Teflon substrate is utilized. The feeding network is designed on the opposite layer of the radiation patch to reduce the influence on the matching from the human body. Based on two different body phantom models, two antenna prototypes were manufactured. They were measured on human body with several separation distances and the resulting shortening effects are discussed. Furthermore, the circuit design for the analysis of the measurement data is presented.

1. INTRODUCTION

These years have witnessed an increasing demand for non-contact and non-invasive detection of biological vital signs such as heartbeat [2]. Moreover, hybrid integration of multi-functions in medical check-up has also been proposed. For example, during CT scans antenna arrays can be buried in the mat and the heartbeat can be detected simultaneously. In this paper, a single patch antenna design for the antenna array implementation to detect the heartbeat signs during medical scans for triggering medical devices is proposed.

BODYNETS 2013, September 30-October 02, Boston, United States

DOI 10.4108/icst.bodynets.2013.253602

Like shown in Fig. 1 the antenna is expected to be between a thin Dartex layer and a foam material in the core of the mat. The Dartex layer and the foam layer compromise the mat on which patients can lie down. The antenna design is subject to several conditions. First, the distance between the antenna and the human body is supposed to be 1 mm or 2 mm, that is the thickness of the Dartex layer, since the patient lies directly on the mat. This means the human body may have a strong shortening effect on the antenna design.

Moreover, an antenna design with broadside radiation is required. Second, the thickness of the metal layers has to be as small as possible. This is because the metal layers influence the measurement results of some medical imagine techniques and the thicker the metal layer, the stronger the influence. To achieve a signal attenuation of lower than 1% in a CT imaging application, a copper layer should be thinner than 5 µm, whereas an aluminium layer could be as thick as 100 µm. Third, the feeding network must be isolated from the influence of the human body; otherwise the matching will be largely deteriorated. Besides, the centre frequency has to be 868 MHz, i. e. the frequency of the short range device (SRD) band in Europe. This band covers the frequency range from 863 MHz to 870 MHz.

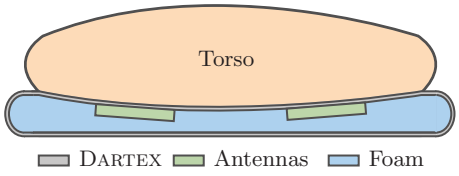

Figure 1: Cross-section of the measurement setup: The patient lies with his back on the mat. The antennas are embedded into the foam and covered by Dartex.

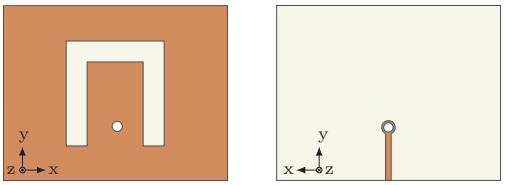

(a) top view (b) bottom view

Figure 2: U-Slot patch antenna design

The paper is organized as follows: First, the initial antenna design is described in details. Moreover, two variants are designed and manufactured. Then, the manufactured antenna prototypes are measured with different setup situations and the performance results are discussed. Afterwards the circuit design for the signal analysis is described and measurement results from the manufactured circuit board are presented. At last, the paper concludes with a summary of the presented results and a description of the following works.

2. ON-BODY ANTENNAS

2.1 Antenna Design

The proposed antenna structure is shown in Fig. 2. The U-slot shape of the antenna patch (in top view) ensures a larger bandwidth than ordinary patch antennas [4, 5]. As illustrated in Fig. 3 a ground plane (layer IV) is positioned on the other side of the ROGERS substrate (layer II) but a Teflon layer with a thickness of 8 mm (layer III) has been inserted in between. This Teflon layer is used to improve the effective bandwidth and the thicker the Teflon layer the higher the bandwidth. Compared with an air-like foam material Teflon has the advantage that the spacing between ground plane and patch is considerably lower.

The feeding microstrip line (layer VI) is on the other side of the ground plane and is etched on a thin copper layer. It feeds the antenna through a via on the ground plane, like Fig. 3 illustrates. This means that the via connects layer I and layer VI. Hence the microstrip feeding line is isolated from the influence of the human body. To prevent a short circuit between via and ground plane a hole with a diameter of 7 mm is located in layer IV. Here the FR4 substrate is not utilized since it has a relatively high variation of the relative permittivity ($4.3 < \varepsilon_r < 4.9$). ROGERS 5000 and 6000 series can provide a stable dielectric performance and moreover they can be delivered with a 9 µm copper cladding which is fairly thin.

The simulation and optimization of the whole patch antenna design are done in HFSS 13. Since the patient lies directly on

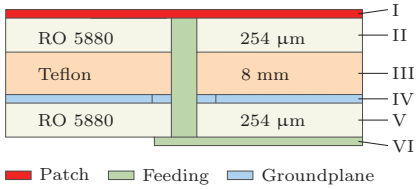

Figure 3: Layer configuration for prototype B

the mat, the patch antenna is in the very near of the human body. The high relative permittivity characteristics of the human body will largely change the antenna characteristics. For narrowband patch antenna, there will be a strong shortening effect on the antenna. This shortening effect is due to the fact that the wave's propagation velocity is reduced in a medium with high permittivity, which results in an shortened effective wavelength [6]. Therefore, the dimension of the antenna has to be downscaled to counteract this effect. The design of the first antenna prototype (A) are based on simulations with a simplified human body phantom model. This phantom is modelled as a cuboid with the dimension $(170 \times 120 \times 200)\,\mathrm{mm}^3$. The human body torso tissue can be approximated using average muscle tissue. The frequency-dependent dielectric parameters of the biological tissues can be referred to [1]. Therefore the phantom has been modelled as a homogeneous cuboid with average relative dielectric constant of 55.1 and average conductivity of 0.9 S/m.

Beside the human body phantom, the influence of the DARTEX layer and the foam layer on the antenna design have also to be considered. In fact, the dielectric characteristics of these two materials were measured using AGILENT 85071E material measurement software and a relative permittivity value of nearly 1 can be concluded for both materials. In combination with the human phantom model the first prototype (A) holds the patch dimension $(35 \times 65)\,\mathrm{mm}^2$ and the substrate dimension $(49 \times 76)\,\mathrm{mm}^2$. This very first antenna is made of a low-cost substrate (ROGERS 4003), because the basic effects of the human body on the antenna characteristic should be investigated as well as the body phantom model verified. In simulations, this antenna shows a resonance frequency at around 868 MHz when placed on the body. Figure 4 shows the measured radiation pattern in free space. The maximum gain is around 7.4 dBi. Due to the absence of the body phantom the matching is shifted to the frequency range of 2.1 GHz to 2.6 GHz. That means the antenna has a bandwidth of approx. 500 MHz in free space.

Like it will be shown in Sec. 2.2 there are significant deviations between simulations and measurements. Therefore a second prototype (B) was designed using an extended human body phantom model. The improved body phantom consists of three layers like Fig. 5 shows. The new antenna design is larger, utilizes an optimized U-slot and has the substrate dimension $(112 \times 132)\,\mathrm{mm}^2$. This final design for on-body use is manufactured as shown in Fig. 6. It uses ROGERS 5880 with a substrate thickness of 254 µm and a 9 µm copper cladding. The microstrip line is connected with a standard SMA connector for feeding. A detailed comparison of both designs is presented in the following section.

2.2 Antenna Measurement Results

The measurement setup can be seen in Fig. 1. For return loss measurements, the in-mat integrated antenna is placed on the right side related to Fig. 1. The antenna characteristics will be verified in the following five different situations for prototype (A):

1. Antenna in free space
2. Antenna in mat, without patient
3. Antenna in mat, patient lying on mat, with T-shirt

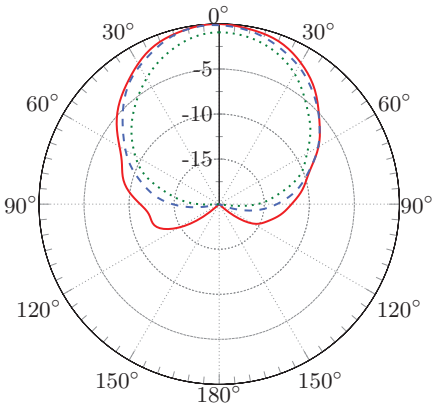

Figure 4: Measured radiation pattern, prototype A, xz-plane, — 2.1 GHz, - - 2.4 GHz, ····· 2.6 GHz

4. Antenna in mat, patient lying on mat, chest bare
5. Antenna direct on patient skin

Fig. 7 shows the return loss of prototype (A). It can be seen that there are clearly differences in the five different situations. The antenna performance in situations (1) air and (2) mat are nearly the same, which implies the influence of the DARTEX and foam materials can be neglected. This agrees with the conclusion from the dielectric permittivity measurements of the DARTEX and foam materials in the previous section. The situations (3) mat + shirt and (4) mat + skin as well as (5) on skin in fact reveal the influence of different spacing distances between antenna and human body on antenna performance.

The shirt textile is some medium with very low relative permittivity so that it holds a dielectric characteristics close to free space. Therefore, the spacing distance between antenna and human body in situation (3) mat + shirt is the thickness of DARTEX layer plus shirt, i. e., around 2 mm. Situation (4) mat + skin have the DARTEX layer between antenna and human body which is approximately 1 mm thick. Situation (5) has the antenna directly touch the human skin, which means 0 mm separation. From Fig. 7 it can be seen that compared with the free space application with a bare chest patient lying on the mat the center frequency is shifted from 2.55 GHz to approx. 1.61 GHz. In case of direct contact with the patient the centre frequency is shifted to 575 MHz.

In short, the smaller the separation distance the stronger the shortening effect. Moreover, the measured resonance frequency is around 575 MHz which is lower than the expected

muscle	$\varepsilon_r = 55.1$
fat	$\varepsilon_r = 5.47$
skin	$\varepsilon_r = 41.58$

Figure 5: Extended body phantom model with three different layers of body tissue

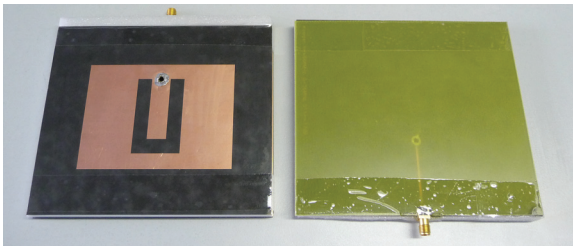

Figure 6: Manufactured final design, prototype B

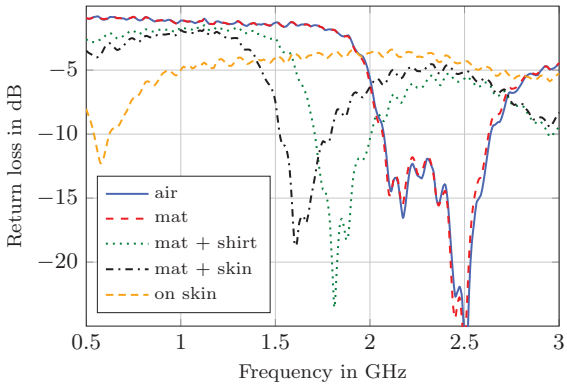

Figure 7: Return loss for different measurement situations for prototype A

868 MHz based on the homogeneous human body phantom. This implies in order to have a more accurate design a more detailed human body phantom should be utilized. Therefore the three-layer torso phantom consisting of skin, fat and muscle layers was designed to take into account the layered structure of the human body. Another parameter that has a strong influence on the return loss is the spacing between skin and antenna surface. Fig. 7 illustrates that a small air gap results in a resonance frequency shift of about 1 GHz. Therefore, considering the results from these measurements, prototype (A) was redesigned.

Like already mentioned the second prototype is an up-scaled version of the first one with modified U-slot geometry and optimized feeding point. It can be seen in Fig. 6. The measurement results based on prototype (B) are shown in Fig. 9 and Fig. 10, respectively. The return loss was measured with two different persons for several positions on the mat. An overview of the different positions is given in Fig. 8. The antennas are integrated in the mat and covered with DARTEX (see Fig. 3). In order to investigate the influence of the antenna position the patients are shifted from the centre to the right side in steps of 2.5 cm. The persons are lying with the dorsum on the mat and wearing a shirt that means it is comparable to situation (3) in Fig. 7. Both measurements yields to a return loss lower than −10 dB at 868 MHz. For all investigated cases the antenna has a bandwidth on the body of at least 100 MHz.

Due to anatomical differences, i. e. the body fat percentage or the body size, each person generates a different mean relative

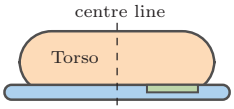

(a) Body in centred position

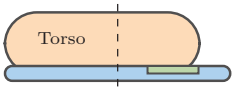

(b) Shift to the left side

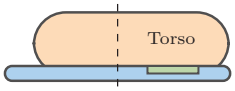

(c) Shift to the right side

Figure 8: Overview of the different positions of the body for the measurement of the return loss

permittivity. In these measurements person 1 has a higher body fat percentage and is larger than person 2. This results in a better contact between skin and the entire antenna surface. For this reasons the return loss changes from person to person. The broadband characteristic of the antenna can compensate such effects to a certain extent. Furthermore, it can be seen that the right shift has only a small influence on the return loss. In this case the antenna is shifted to the centre of the dorsum, which makes not much difference with regard to the electrical properties of the surrounding medium.

In contrast a shift to the left side has a bigger impact. That is due to the fact that the antenna is shifted to the edge of the body. For a value of −7.5 cm the influence of the free space is noticeable, which results in a higher resonance frequency. Another reason is the increasing curvature of the body at the edge of the costal arch, which leads to lower contact between skin and antenna. This behaviour is clearly recognizable in Fig. 10b. Because person 2 is smaller than person 1 for a shift of −7.5 cm the antenna is no longer completely covered by the body, which results in a return loss considerably worse than −10 dB.

An even higher bandwidth can be realized with the use of carbon instead of copper. Besides, this configuration has the advantage that no disturbing metal layers exist. On the other side there are higher losses.

3. CIRCUIT DESIGN

3.1 System Concept

The proposed system concept of the Doppler radar is shown in Fig. 11. Due to differences in the permittivity of the cardiac muscle and the surrounding tissue, a part of the

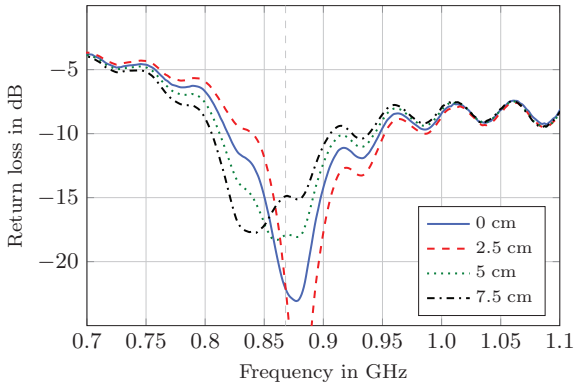

(a) Shift from the centre line of the mat to the right side

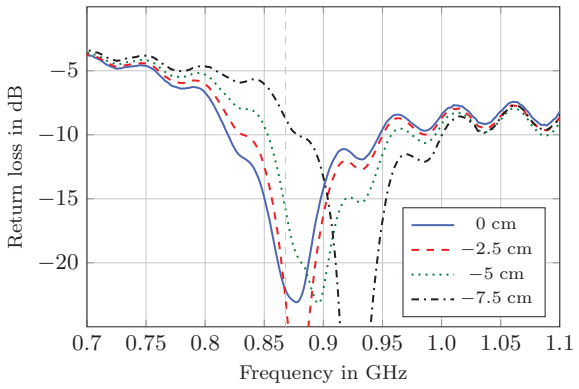

(b) Shift from the centre line of the mat to the left side

Figure 9: Measured return loss for the final design (prototype B) and patient 1

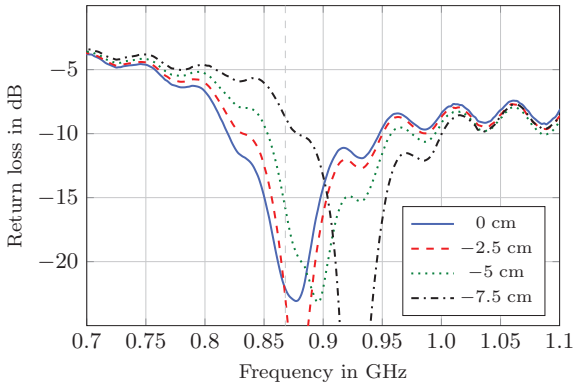

(a) Shift from the centre line of the mat to the right side

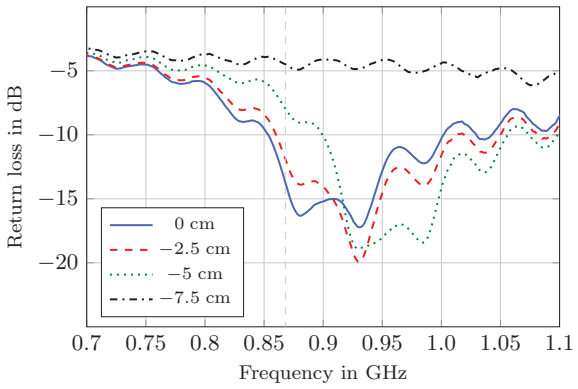

(b) Shift from the centre line of the mat to the left side

Figure 10: Measured return loss for the final design (prototype B) and patient 2

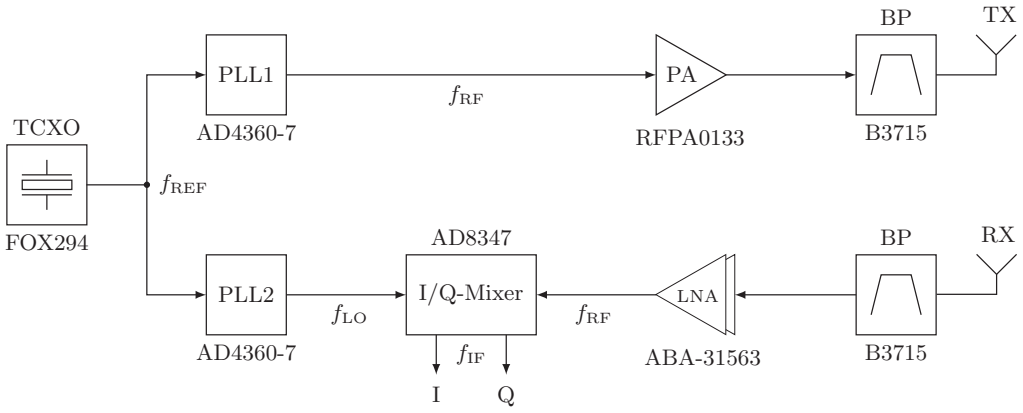

Figure 11: System block diagram of the proposed front-end. The transmitting and receiving antenna are integrated into the mat and have a Dartex cover.

transmitted wave is reflected at the boundary layer. The reflected part is received by the second antenna. The periodically time varying displacement of the heart results in a phase modulation (PM). The analysis of the PM enables the determination of the heartbeat.

The circuit consists of two correlated synthesizer components PLL1 and PLL2, which can independently generate continuous wave (CW) signals, and a quadrature demodulator. The RF power amplifier, the low noise amplifier (LNA) and the additional filters enhance both the signal level and the signal spectral purity. The detection of the heartbeat is based on the principle that a target with a periodic movement, in this case the heart, modulates the phase of the reflected CW-signal proportionally to its time-varying position.

The single-tone signal $T(t)$ from Eq. (1) with the oscillation frequency f, the elapsed time t and the phase noise $\varphi(t)$ of the oscillator of the first synthesizer is amplified in the forward path.

$$T(t) = \cos(2\pi f t) + \varphi(t) \tag{1}$$

A surface acoustic wave (SAW) bandpass filter suppress the distortion products. The transmit signal is software selectable available with 5 dBm, 16 dBm, 23 dBm or 27 dBm at the interface to the antenna. The use of a phase-locked loop (PLL) instead of a simple voltage-controlled oscillator (VCO) enhances the frequency stability. The usage of the direct synthesis approach makes additional mixers in the transmit path superfluous. The nominal distance between the antenna and the heart is referred to as d_0. The wave is reflected at the surface of the heart and is phase modulated through the movement $x(t)$ of the cardiac muscle. The phase modulation for these human vital sign is detectable in the range of 0.05 Hz to 10 Hz. The upper limit is determined by the used low pass filter. The attenuation of the CW signal between transmitter and receiver is approximately 40 dB due to absorption in the dielectric materials, polarization mismatch, reflections and antenna losses.

The received signal $R(t)$ is pre-amplified with a LNA and passed to the I/Q mixer. According to [3] it can be approximated as seen in Eq. (2) if the heart moves with a period of $T \gg {}^{d_0}/_{c}$ and the shift of the moving heart is $x(t) \ll d_0$ where the wavelength is $\lambda = {}^{c}/_{f}$.

$$R(t) \approx \cos\left[2\pi f t - \frac{4\pi d_0}{\lambda} - \frac{4\pi x(t)}{\lambda} + \varphi\left(t - \frac{2d_0}{c}\right)\right] \tag{2}$$

By demodulating the phase of the received signal the rates are retrieved. The local oscillator (LO) signal for the demodulator is generated by the second synthesizer. The frequency difference between both synthesizer components, which are fed from the same temperature compensated crystal oscillator (TCXO), determines the intermediate frequency (IF) of the receiver output. I- and Q-channels are differential signals with a commode mode voltage of 1 V and a maximum differential amplitude of 760 mV. Both outputs have an internal DC-compensation which leads to a highpass characteristic with a corner frequency of approx. 40 Hz. Further there is an automatic gain control (AGC) integrated into the I/Q demodulator. The signals of the two output channels can be written down as shown in [3].

$$B_{\mathrm{I}}(t) = \cos\left(\vartheta + \frac{\pi}{4} + \frac{4\pi x(t)}{\lambda} + \Delta\varphi(t)\right) \tag{3}$$

$$B_{\mathrm{Q}}(t) = \cos\left(\vartheta - \frac{\pi}{4} + \frac{4\pi x(t)}{\lambda} + \Delta\varphi(t)\right) \tag{4}$$

The variable ϑ represents the constant phase shift due to the distance d_0 and the offset ϑ_0.

$$\vartheta = \frac{4\pi d_0}{\lambda} + \vartheta_0 \tag{5}$$

The other option is the direct conversion mode and the use of the power detector. The output voltage of the power detector has a range of 0.2 V to 1 V. Where 0.2 V corresponds to an input power level of −80 dBm and 1 V to an input power of −10 dBm. The AGC bandwidth is approx. 0.5 Hz. If both synthesizers are set to equal frequencies the receiver works as a direct conversion receiver. After lowpass-filtering the baseband signal $B(t)$ is [3]:

$$B_{\mathrm{LPF}}(t) \approx \cos\left(\frac{4\pi d_0}{\lambda} + \frac{4\pi x(t)}{\lambda} + \vartheta_0 + \Delta\varphi(t)\right) \tag{6}$$

Table 1: Main operation parameters of the radar front-end

Parameter	Min.	Typ	Max.	Unit
Frequency	868		870	MHz
Supply voltage	6		12	V
Current drawn			500	mA
Ouput power	5	12	25	dBm
Input power	-80		-10	dBm
I/Q common mode		1		V
IF frequency	0.1		10	MHz

where the residual phase noise

$$\Delta\varphi(t) = \varphi(t) - \varphi\left(t - \frac{2d_0}{c}\right) \tag{7}$$

is dependent on the level of correlation between $R(t)$ and LO and is greatly reduced due the small distance between the antennas and the moving heart. In this operation mode the amplitude of the output voltage is proportional to the phase-shift between transmitted and received signal if the radar target is within the unambiguous range. Slow phase changes can be better detected with the power detector output of the AGC, otherwise the AGC and the DC-compensation would compensate slow changes of the output amplitude due to the pronounced highpass behaviour. The radar front-end achieves the operating parameters listed in Tab. 1.

3.2 Implementation

The demonstrator is implemented on a 1.5 mm thick FR4 4-layer stack-up with two signal layers, one ground and one power plane. The prototype board is partitioned into RF parts with impedance-controlled 50 Ω lines and additional analog, power management and digital circuitry. The design of the PLLs VCO power supply was made with special care to prevent any unintended modulation or pulling of the integrated VCOs from other on-board components. Therefore the VCOs have their own voltage controllers whose bypass capacitors are crucial to the rejection of power supply ripple. The final circuit layout for the top signal layer is shown in Fig. 13. The microcontroller unit labelled IC1 on the upper left side of the board is used to program the output frequencies of the PLLs. The printed circuit board is powered from a single 6 V to 12 V power supply and integrates connectors for interfacing of the receive (RX) and transmit (TX) antennas and the in- and quadrature-phase outputs of the I/Q demodulator for further digital signal processing.

3.3 Measurement Results

First time domain measurements have been carried out with two of the previously mentioned antennas (prototype B) operating in the 869 MHz band and a digital oscilloscope during the radar front-end was in IF mode. The antennas are matched to the body tissue and were placed directly on the clothing. The waveform without any further signal processing can be seen in Fig. 12a. In this case the heartbeat is difficult to detect. Therefore additional signal processing is necessary.

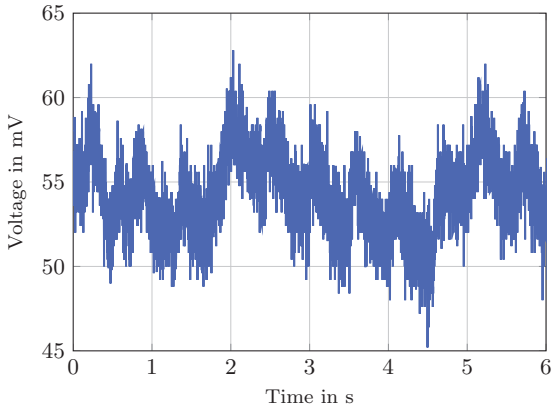

(a) Time domain measurement of the heartbeat rate with prototype B using the IF operation mode.

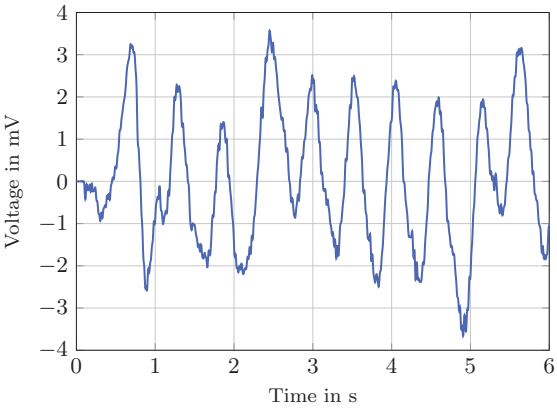

(b) Post-processed time domain measurement of the heartbeat rate with prototype B using the IF operation mode. The 0.55 s spaced peaks correspond to a heartbeat rate of 1.8 Hz.

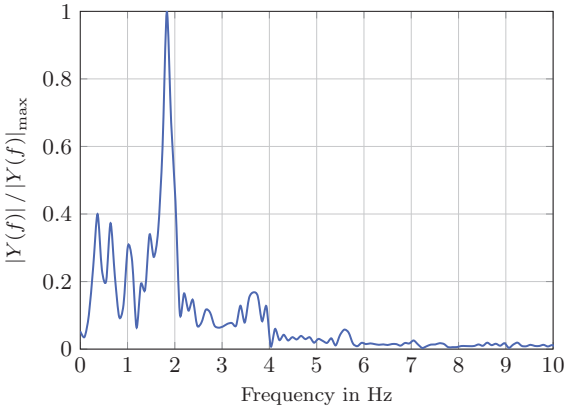

(c) Normalized frequency spectrum calculated from the time domain measurements of Fig. 12b

Figure 12: Measured and post-processed time signal with the final design (prototype B)

The signal processing was conducted externally with the measurement equipment and could be divided into the following steps:

1. applying a higher order bandpass filter in the expected heartbeat range,
2. windowing and autocorrelation of the signal to get the periodic heartbeat signal and
3. Fast Fourier Transform (FFT) the signal to obtain the heartbeat rate.

The post-processed signal is shown in Fig. 12b and Fig. 12c, respectively. Now the heartbeat is detectable from the periodic amplitude changes in Fig. 12b as well as the frequency spectrum. The 0.55 s spaced peaks in the diagram correspond to a heartbeat rate of 109 bpm. This is also recognizable in Fig. 12c which has a peak at approx. 1.8 Hz. The heartbeat rate is higher than the standard value due to the fact that the measurements were accomplished after light sportive activities. In Fig. 12c there are also some small peaks around 0.5 Hz which could be caused by breathing.

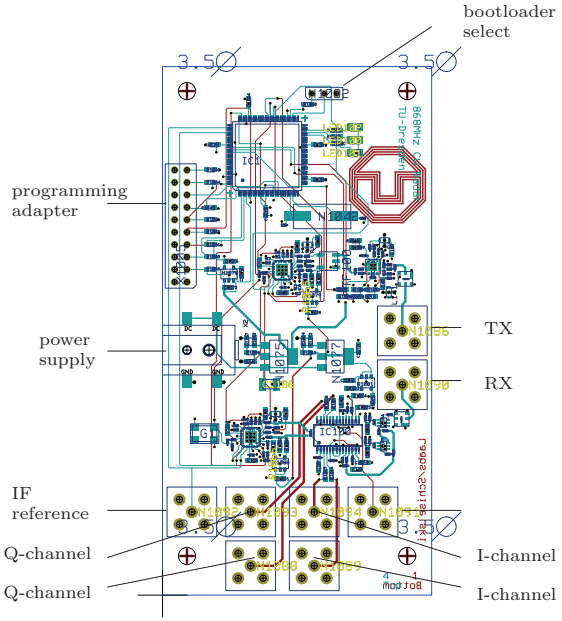

Figure 13: Circuit board layout of the proposed demonstrator

4. CONCLUSIONS

This paper describes a single patch antenna design operating in 868 MHz band for the antenna array implementation to detect the patient heartbeat during medical scans for triggering medical devices. Considering the influence of the thickness of copper cladding on the quality of medical imaging techniques, two different variants are manufactured and measured in different situations. Human body shortening effect on the antenna design has been fully discussed. The Doppler radar concept combined with digital signal processing techniques offer an effective non-invasive remote sensing of human vital signs in medical applications. Especially systems in the sub-GHz range are promising because of low costs for the RF components and reduced damping and attenuation through blankets or mats. The proposed demonstrator supports a direct conversion and a heterodyne operation mode.

5. REFERENCES

[1] Italien National Research Council, Institute for Applied Physics. Dielectric Properties of Body Tissues. URL: `http://niremf.ifac.cnr.it/tissprop/htmlclie/htmlclie.htm`, May 2013.

[2] L. Chioukh, H. Boutayeb, K. Wu, and D. Deslandes. Monitoring vital signs using remote harmonic radar concept. In *Radar Conference (EuRAD), 2011 European*, pages 381–384, 2011.

[3] A. Droitcour, O. Boric-Lubecke, V. Lubecke, J. Lin, and G. Kovacs. Range correlation and i/q performance benefits in single-chip silicon doppler radars for noncontact cardiopulmonary monitoring. *Microwave Theory and Techniques, IEEE Transactions on*, 52(3):838–848, 2004.

[4] K.-F. Lee, K. Luk, K. F. Tong, Y. L. Yung, and T. Huynh. Experimental study of the rectangular patch with a u-shaped slot. In *Antennas and Propagation Society International Symposium, 1996. AP-S. Digest*, volume 1, pages 10–13 vol.1, 1996.

[5] K. F. Tong, K. Luk, and K.-F. Lee. Design of a broadband u-slot patch antenna on a microwave substrate. In *Microwave Conference Proceedings, 1997. APMC '97, 1997 Asia-Pacific*, volume 1, pages 221–224 vol.1, 1997.

[6] Q. Wang, K. Wolf, and D. Plettemeier. An uwb capsule endoscope antenna design for biomedical communications. In *Applied Sciences in Biomedical and Communication Technologies (ISABEL), 2010 3rd International Symposium on*, pages 1–6, 2010.